A projected approximation to strongly contracted N-electron valence perturbation theory for DMRG wavefunctions

Michael Roemelt, Sheng Guo, and Garnet K.-L. Chan'

Citation: J. Chem. Phys. **144**, 204113 (2016); doi: 10.1063/1.4950757
View online: http://dx.doi.org/10.1063/1.4950757
View Table of Contents: http://aip.scitation.org/toc/jcp/144/20
Published by the American Institute of Physics

A projected approximation to strongly contracted N-electron valence perturbation theory for DMRG wavefunctions

Michael Roemelt,[1,2,3] Sheng Guo,[1] and Garnet K.-L. Chan[1,a)]
[1]*Frick Laboratory, Department of Chemistry, Princeton University, Princeton, New Jersey 08544, USA*
[2]*Lehrstuhl für Theoretische Chemie, Ruhr-Universität Bochum, D-44789 Bochum, Germany*
[3]*Max-Planck Institut für Kohlenforschung, Kaiser-Wilhelm Platz 1, D-45470 Mülheim an der Ruhr, Germany*

(Received 3 March 2016; accepted 4 May 2016; published online 26 May 2016)

A novel approach to strongly contracted N-electron valence perturbation theory (SC-NEVPT2) as a means of describing dynamic electron correlation for quantum chemical density matrix renormalization group (DMRG) calculations is presented. In this approach the strongly contracted perturber functions are projected onto a renormalized Hilbert space. Compared to a straightforward implementation of SC-NEVPT2 with DMRG wavefunctions, the computational scaling and storage requirements are reduced. This favorable scaling opens up the possibility of calculations with larger active spaces. A specially designed renormalization scheme ensures that both the electronic ground state and the perturber functions are well represented in the renormalized Hilbert space. Test calculations on the N_2 and $[Cu_2O_2(en)_2]^{2+}$ demonstrate some key properties of the method and indicate its capabilities. *Published by AIP Publishing.* [http://dx.doi.org/10.1063/1.4950757]

I. INTRODUCTION

Describing complex molecular systems such as transition metal complexes or extended conjugated π-systems with quantitative accuracy is one of the greatest challenges in electronic structure theory. Many of these systems require a multiconfigurational treatment that properly takes into account static electron correlation effects. The most widely used approaches to capture static electron correlation effects are the complete active space self-consistent field (CASSCF) and complete active space configuration interaction (CASCI) methods. As they both solve the full configuration interaction (full-CI) problem within a finite active space they provide the required flexibility to yield a qualitatively correct wavefunction.[1] Quantitative accuracy, however, is only reached if dynamic electron correlation effects are considered, too. Hence, a number of ways to treat dynamic electron correlation on top of CASSCF and CASCI have been proposed and established over the years including multiple flavors of configuration interaction (CI), perturbation theory (PT), and coupled cluster theory (CC).[2–7] A common concern of all of these methods is their computational cost. With increasing number of strongly correlated electrons (and also system size) the underlying CASSCF and CAS-CI calculations become infeasible.[1] In such situations one must either rely on single-determinant based methods such as density functional theory (DFT) or make approximations to the full-CI solution within the active orbital space as, for example, provided by the widely used restricted active space SCF method (RASSCF).[8,9] In the last decade the *ab initio* density matrix renormalization group (DMRG) has been shown to provide another reasonable and accurate alternative to complete active space methods.[10–21] It can be regarded as an approximation to the exact diagonalization of the large Hamiltonian matrix in the basis of many-electron wavefunctions within the active orbital space. A great advantage of DMRG is that it approximately solves a problem whose complexity scales exponentially with increasing system size by optimizing only a polynomial number of parameters. Owing to this favorable behavior DMRG is able to treat large active spaces on the order of 20-80 orbitals.[22–29]

Treating dynamic electron correlation on top of large-scale DMRG calculations is currently an active field of research. It is possible to straightforwardly implement direct analogues of multi-reference dynamic correlation methods on top of DMRG wavefunctions. This has given rise to methods such as DMRG-CAS-PT2,[30] DMRG-MRCI,[31,32] and DMRG-SC-NEVPT2.[33] However, none of these methods are yet able to deal with the very largest active spaces accessible to DMRG. At the heart of the problem is the amount of information about the active space that is required as input to dynamic electron correlation calculations. Even rather simple approximations such as internally contracted CAS-PT2 require the evaluation of active space density matrices of up to fourth order.[3,4,30] For the aforementioned active space sizes a straightforward calculation of these quantities quickly becomes prohibitive. Therefore a number of approximate schemes have been introduced in recent years where the complexity and amount of required information about the active space are reduced.[34] For example, canonical transformation (CT) theory which was introduced by Chan and Yanai discards all density matrices of higher than second order.[35–38] In Zgid and Chan's cumulant version of SC-NEVPT2 and Yanai's cumulant versions of DMRG-CASPT2 and DMRG-MRCI higher order density matrices are approximated by lower rank cumulant expansions.[31,39] A different route was taken in Sharma's recent MPS-PT2 and MPS-linear coupled cluster

a)Author to whom correspondence should be addressed. Electronic mail: gkc1000@gmail.com

(MPS-LCC) methods where all states outside the active space that contribute to the electronic ground state are approximated as a matrix product state (MPS) which greatly reduces the complexity of the problem.[40,41] A combination of DMRG with block correlated second order perturbation theory starting from a GVB reference was proposed by Li *et al.*[42,43] Also, Sokolov and Chan recently used a time-dependent formulation which bypasses the need for a contracted formulation and avoids 4-particle density matrices.[44] An alternative is to forgo using the DMRG wavefunction as the reference or to use simpler dynamic correlation methods. For example, Reiher has recently published works where DMRG has been combined with DFT in a range separated Ansatz as well as an embedding scheme.[45,46] All of the aforementioned methods feature different tradeoffs between accuracy and computational feasibility that allows them to treat differently sized systems with varying accuracy.

In this work we present a novel approach to the combination of DMRG and strongly contracted second order N-electron valence perturbation theory (SC-NEVPT2) for quantum chemical multireference calculations.[5,6] The main objective of this approach is to lower the cost to treat systems with large active spaces and large orbital spaces with a moderate and controllable accuracy. The complexity of the problem and the computational cost are reduced by projecting the perturber functions as well as the unperturbed Hamiltonian onto a reduced Hilbert space. The form of this reduced space is determined by a modified density matrix renormalization procedure. This procedure ensures that both the electronic ground state and the perturber functions are accurately approximated during the calculation. We use test calculations on the nitrogen dimer and $[Cu_2O_2(en)_2]^{2+}$ to demonstrate the properties of the presented method as a way of describing dynamical electron correlation in large multireference systems.

II. THEORY

This section will be divided into three subsections. Sections II A and II B comprise brief recapitulations of the DMRG algorithm in multireference quantum chemistry and the SC-NEVPT2 method, respectively. Eventually, Section II C outlines the framework of the presented combination of both methods. In the following the total orbital space is decomposed into three subspaces containing internal (core), active, and external (virtual) orbitals. Internal orbitals are labelled i, j, k, l while active orbitals are denoted by orbital labels t, u, v, w and external orbitals carry labels a, b, c, d. Orbital labels p, q, r, and s refer to general orbitals.

A. Matrix product states and the DMRG algorithm

The main focus of this work is on the novel combination of SC-NEVPT2 with *ab initio* DMRG calculations. Hence, this section highlights only some key features of matrix product states (MPS's) and the density matrix renormalization group that are relevant for the present work. For more detailed information we refer to a number of reviews about the application of MPS's and DMRG in quantum chemistry.[12,25,47–49] In molecular *ab initio* DMRG calculations, the DMRG algorithm is used to approximate the full-CI solution within the active orbital space. For this purpose, the k (usually localized) active orbitals are projected on a one-dimensional lattice as depicted in Figure 1. In this scheme, each active orbital is represented by a single site on the lattice. Without going into any further detail we just note that the order of the active orbitals on the one-dimensional lattice is a critical aspect of the procedure and that a number of strategies to determine suitable orders exist.[50–52] Once a suitable order has been found the active space wavefunction is approximated as a MPS according to

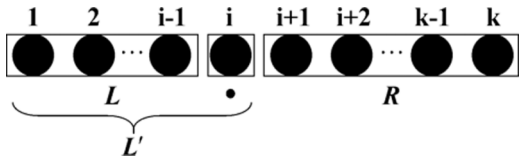

FIG. 1. The arrangement of the active orbitals 1 to k on a one-dimensional lattice and their division into three blocks $\boldsymbol{L}$, $\boldsymbol{R}$, and •. During the blocking step $\boldsymbol{L}$ and • form the new block $\boldsymbol{L}'$.

$$|\Psi_{MPS}\rangle = \sum_{n} \boldsymbol{A}^{n_1}\boldsymbol{A}^{n_2}\cdots\boldsymbol{A}^{n_k}\,|\boldsymbol{n}\rangle\,. \tag{1}$$

Here, $|\boldsymbol{n}\rangle = |n_1 n_2 \cdots n_k\rangle$ is the occupation number representation of any active space Slater determinant or configuration state function. The expansion coefficients in Equation (1) are computed as products of local site tensors $\boldsymbol{A}_t$. For any given orbital occupation n_t, $\boldsymbol{A}_t^{n_t}$ is a $M \times M$ matrix and each $\boldsymbol{A}_t$ is correspondingly a three-index tensor. The first and last local site tensors are special as the dimensions of $\boldsymbol{A}_1^{n_1}$ and $\boldsymbol{A}_k^{n_k}$ are $1 \times M$ and $M \times 1$, respectively. M is a preset parameter usually referred to as the bond dimension, contraction depth, or number of kept states. As the bond dimension M determines the flexibility of the expansion coefficients, it also regulates the accuracy of the approximation with higher values of M corresponding to a more accurate approximation. For a given MPS the DMRG ground state algorithm can be regarded as a way to optimize the local site tensors $\boldsymbol{A}_t^{n_t}$.

The DMRG algorithm is an iterative procedure that successively optimizes the local site tensors at adjacent sites on the lattice. During each iteration the local site tensor for a specific site is optimized in three steps: (i) *blocking*, (ii) *solution of the Schrödinger equation*, and (iii) *renormalization*. The *blocking* step involves the division of the lattice into three blocks: the left block **L** ranging from site 1 to $t-1$, the right block **R** consisting of sites $t+1$ to k, and the so called dot-block • on site t (Figure 1). Note that this division pattern corresponds to the "one-site" flavor of the DMRG. As the "one-site" algorithm tends to converge to local minima, all presented calculations employ the more stable and robust "two-site" algorithm, which is explained in detail elsewhere,[10] until convergence is (almost) reached and then switch to the "one-site" algorithm. When the t'th local site tensor is optimized during the "one-site" algorithm it is advantageous to write the MPS from Equation (1) in its t'th canonical representation,

$$\left|\Psi^{(t)}_{MPS}\right\rangle = \sum_{n_1 n_2 n_3 \cdots n_N} \boldsymbol{L}^{n_1}\boldsymbol{L}^{n_2}\cdots\boldsymbol{L}^{n_{t-1}}\boldsymbol{C}^{n_t}\boldsymbol{R}^{n_{t+1}}\cdots\boldsymbol{R}^{n_N} \times |n_1 n_2 n_3 \cdots n_N\rangle = \sum_{l_t n_t r_t} C_{l_t n_t r_t} |l_t n_t r_t\rangle . \quad (2)$$

Here, all local site tensors on the left side of site t are denoted as $\boldsymbol{L}^{n_P}$ whereas all local site tensors on the right side of t are labelled $\boldsymbol{R}^{n_P}$. In the context of DMRG the matrices $\boldsymbol{L}^{n_P}$ and $\boldsymbol{R}^{n_P}$ are sometimes referred to as left and right rotation matrices and they satisfy the orthonormality relations $\sum_{n_P} \boldsymbol{L}^{n_P T}\boldsymbol{L}^{n_P} = \mathbf{1}$ and $\sum_{n_P} \boldsymbol{R}^{n_P T}\boldsymbol{R}^{n_P} = \mathbf{1}$. These matrices contain the essential information about the renormalization process (*vide infra*). In the second line of Equation (2), all left rotation matrices are contracted and together with the set of Fock states $\{|n_1 n_2 n_3 \cdots n_{t-1}\rangle\}$ form a M-dimensional set of functions $\{|l_t\rangle\}$ that is associated with the left block. An analogous M-dimensional set of functions $\{|r_t\rangle\}$ is constructed on the right block through contraction of all right rotation matrices. Accordingly, the expansion coefficients in the t'th canonical representation (second line of Equation (2)) feature three indices. The expansion coefficient matrices of canonical representations belonging to adjacent sites t and $t+1$ can be interconverted according to

$$\boldsymbol{L}^{n_{t-1}T}\boldsymbol{C}^{n_t}\boldsymbol{R}^{n_{t+1}} = \boldsymbol{C}^{n_{t+1}}. \quad (3)$$

After division of the lattice into the three blocks and the formation of the corresponding sets of functions, the direct product space of $\{|l_t\rangle\}$ and $\{|n_t\rangle\}$ is formed,

$$\left\{\left|l'_t\right\rangle\right\} = \{|l_t\rangle\} \otimes \{|n_t\rangle\} . \quad (4)$$

Accordingly, $\left|\Psi^{(t)}_{MPS}\right\rangle$ is expanded as

$$\left|\Psi^{(t)}_{MPS}\right\rangle = \sum_{l'_t r_t} C_{l'_t r_t} \left|l'_t r_t\right\rangle . \quad (5)$$

In the second step, the electronic Schrödinger equation $\boldsymbol{HC} = \boldsymbol{EC}$ is set up in the direct product basis $\left\{\left|l'_t\right\rangle\right\} \otimes \{|r_t\rangle\}$ and solved using standard quantum chemical tools such as the Davidson or Lanczos diagonalization schemes.[53,54] As a result, the approximate electronic ground state Ψ_0 and its corresponding total energy are obtained as the lowest root of the electronic Hamiltonian matrix $\boldsymbol{H}$. Step (iii) features the renormalization of $\left\{\left|l'_t\right\rangle\right\}$ by means of a singular value decomposition (SVD) of the traced reduced ground state density matrix

$$\hat{D}_L = tr_r |\Psi_0\rangle\langle\Psi_0| . \quad (6)$$

In this way, the M most important states for the description of Ψ_0 that can be formed from elements in $\left\{\left|l'_t\right\rangle\right\}$ are identified. These M states form the renormalized basis $\left\{\left|l^{renorm}_t\right\rangle\right\}$. Moreover, the SVD of $\hat{D}_L$ yields the rotation matrix $\boldsymbol{L}^{n_t}$ as the mapping from $\left\{\left|l'_t\right\rangle\right\}$ to $\left\{\left|l^{renorm}_t\right\rangle\right\}$ which is in turn used to set up the left basis for site $t+1$ in the next *blocking* step, hence $\left\{\left|l^{renorm}_t\right\rangle\right\} = \{|l_{t+1}\rangle\}$. Of course, it is also possible to perform the SVD with the density of any other state obtained from the preceding diagonalization step or the density of a weighted sum of states. In this way one can optimize the rotation matrices for the description of an excited state or multiple excited states simultaneously. In any case, steps (i)–(iii) are repeated for adjacent sites until the end of the lattice is reached. A complete set of iterations for the entire lattice is called a sweep. Once a sweep in one direction has been completed, a sweep in the opposite direction is started using the left rotation matrices as right rotation matrices and vice versa. A complete DMRG calculation consists of multiple forward and backward sweeps until convergence of the total energy is reached. It is important to note that when the "one-site" scheme is applied and the point of convergence is reached the form of the ground state wavefunction is left unchanged throughout an entire sweep. Hence, the k canonical representations are equivalent $4M^2$-dimensional representations of the same wavefunction.

Construction of the secular equation $\boldsymbol{HC} = \boldsymbol{EC}$ in step (ii) of a DMRG iteration requires the evaluation of matrix elements of the electronic Hamiltonian which in second quantization reads as

$$\hat{H} = \sum_{pq} h_{pq}\hat{a}^\dagger_p\hat{a}_q + \frac{1}{2}\sum_{pqrs}(pq\,|\,rs)\,\hat{a}^\dagger_p\hat{a}^\dagger_r\hat{a}_s\hat{a}_q . \quad (7)$$

Here, h_{pq} and $(pq\,|\,rs)$ are molecular one- and two-electron integrals and $\hat{a}^\dagger_p$ and $\hat{a}_q$ are fermion creation and annihilation operators, respectively. If the indices of the two electron operator $\hat{a}^\dagger_p\hat{a}^\dagger_r\hat{a}_s\hat{a}_q$ are distributed over two different blocks, its matrix elements can be evaluated as a product of local matrix elements in the basis of the different blocks. For example, if sites (orbitals) p and r are located on the left block while sites q and s are located on the right block, the matrix element of $\hat{a}^\dagger_p\hat{a}^\dagger_r\hat{a}_s\hat{a}_q$ between the two functions $\Phi_I = l'_{t,1} \otimes r_{t,1}$ and $\Phi_J = l'_{t,2} \otimes r_{t,2}$ can then be written as

$$\langle\Phi_I|\,\hat{a}^\dagger_p\hat{a}^\dagger_r\hat{a}_s\hat{a}_q\,|\Phi_J\rangle = \left\langle l'_{t,1}r_{t,1}\right|\hat{a}^\dagger_p\hat{a}^\dagger_r\hat{a}_s\hat{a}_q\left|l'_{t,2}r_{t,2}\right\rangle = \left\langle l'_{t,1}\right|\hat{a}^\dagger_p\hat{a}^\dagger_r\left|l'_{t,2}\right\rangle\left\langle r_{t,1}\right|\hat{a}_s\hat{a}_q\left|r_{t,2}\right\rangle . \quad (8)$$

Analogous equations can be formulated for operators whose indices are distributed over other pairs of blocks, e.g., the left and the dot block. During the blocking step of each iteration of the DMRG algorithm one- and two-index operator matrices of the form $\left\langle l'_{t,1}\right|\hat{a}^\dagger_p\left|l'_{t,2}\right\rangle$, $\left\langle l'_{t,1}\right|\hat{a}^\dagger_p\hat{a}_q\left|l'_{t,2}\right\rangle$, and $\left\langle l'_{t,1}\right|\hat{a}^\dagger_p\hat{a}^\dagger_q\left|l'_{t,2}\right\rangle$ are generated on the left and right block. In this work, the aforementioned operators are generated and used in their spin-adapted form as described by Sharma and Chan.[55]

B. N-electron valence perturbation theory

Second order N-electron valence perturbation theory (NEVPT2), introduced by Angeli *et al.* in 2001, is now established as a standard method to introduce dynamic electron correlation into multireference quantum chemical calculations.[5,6] Generally, NEVPT2 follows the "diagonalize and perturb" approach to multireference perturbation theory and its starting point is an unperturbed wavefunction $\Psi^{(0)}_m$ together with the corresponding Hamiltonian $\hat{H}_0$ that results

from a preceding active space calculation,

$$\begin{aligned} \left|\Psi_m^{(0)}\right\rangle &= \sum_I^{CAS} c_I \left|\Phi_I\right\rangle, \\ \hat{H}_0 &= \hat{P}^{CAS}\hat{H}\hat{P}^{CAS}, \\ \hat{H}_0\left|\Psi_m^{(0)}\right\rangle &= E_m\left|\Psi_m^{(0)}\right\rangle. \end{aligned} \tag{9}$$

Here, the index m indicates that $\Psi_m^{(0)}$ is the m'th root of the secular system of equations defined by the CASSCF problem and E_m denotes the energy eigenvalue corresponding to $\Psi_m^{(0)}$. Furthermore, it is implied that $\Psi_m^{(0)}$ features n_v active electrons and n_c inactive electrons.

The space of perturber functions for NEVPT2 is defined as the first order interacting space (FOIS) which is generated by the action of $\hat{H}$ on the reference function $\Psi_m^{(0)}$. Any function $\Psi_\mu^{(n_k),\lambda}$ contained in the FOIS can be written as a direct product of two functions, i.e., $\Psi_\mu^{(n_k),\lambda} = \Psi_\mu^{n_v+n_k} \otimes \Phi_\lambda^{-n_k}$, where $\Psi_\mu^{n_v+n_k}$ is the μ'th multireference function describing the active orbital part with $n_v + n_k$ electrons and $\Phi_\lambda^{-n_k}$ is an orbital product of inactive orbitals where n_k electrons have been removed. In this notation λ denotes the fixed occupation pattern of the inactive orbitals of $\Psi_\mu^{(n_k),\lambda}$. The subspace of all perturber functions with a given inactive occupation pattern λ and number of transferred electrons n_k will be referred to as $S_\lambda^{(n_k)} = \left\{\Psi_\mu^{(n_k),\lambda}\right\}$. In the strongly contracted form of NEVPT2 each $S_\lambda^{(n_k)}$ is represented by a single function, $\Psi_\lambda^{(n_k)}$, that is simply the sum of all functions contained in $S_\lambda^{(n_k)}$. More precisely,

$$\left|\Psi_\lambda^{(n_k)}\right\rangle = \hat{V}_\lambda^{(n_k)}\left|\Psi_m^{(0)}\right\rangle = P^{S_\lambda^{(n_k)}}\hat{H}\left|\Psi_m^{(0)}\right\rangle, \tag{10}$$

where eight different classes of operators $\hat{V}_\lambda^{(n_k)}$ can be defined[6]

$$\begin{aligned}
\hat{V}^{(0)}_{ij,ab} &= \gamma_{ij}\gamma_{ab}\sum_{\sigma\tau}^{-1/2,1/2}\left\{(ia\,|\,jb)\,\hat{a}^\dagger_{a\sigma}\hat{a}_{i\sigma}\hat{a}^\dagger_{b\tau}\hat{a}_{j\tau} + (ja\,|\,ib)\,\hat{a}^\dagger_{a\sigma}\hat{a}_{i\sigma}\hat{a}^\dagger_{b\tau}\hat{a}_{i\tau}\right\} \quad i\le j,\ a\le b, \\
\hat{V}^{(-1)}_{ab,i} &= \gamma_{ab}\sum_{t}^{active}\sum_{\sigma\tau}^{-1/2,1/2}\left\{(ia\,|\,tb)\,\hat{a}^\dagger_{a\sigma}\hat{a}_{i\sigma}\hat{a}^\dagger_{b\tau}\hat{a}_{t\tau} + (ja\,|\,ib)\,\hat{a}^\dagger_{a\sigma}\hat{a}_{t\sigma}\hat{a}^\dagger_{b\tau}\hat{a}_{i\tau}\right\} \quad a\le b, \\
\hat{V}^{(1)}_{ij,a} &= \gamma_{ij}\sum_{t}^{active}\sum_{\sigma\tau}^{-1/2,1/2}\left\{(ia\,|\,jt)\,\hat{a}^\dagger_{a\sigma}\hat{a}_{i\sigma}\hat{a}^\dagger_{t\tau}\hat{a}_{j\tau} + (ja\,|\,it)\,\hat{a}^\dagger_{a\sigma}\hat{a}_{j\sigma}\hat{a}^\dagger_{t\tau}\hat{a}_{i\tau}\right\} \quad a\le b, \\
\hat{V}^{(-2)}_{ab} &= \gamma_{ab}\sum_{tu}^{active}\sum_{\sigma\tau}^{-1/2,1/2}(ta\,|\,ub)\,\hat{a}^\dagger_{a\sigma}\hat{a}_{t\sigma}\hat{a}^\dagger_{b\tau}\hat{a}_{u\tau} \quad a\le b, \\
\hat{V}^{(2)}_{ij} &= \gamma_{ij}\sum_{tu}^{active}\sum_{\sigma\tau}^{-1/2,1/2}(it\,|\,ju)\,\hat{a}^\dagger_{t\sigma}\hat{a}_{i\sigma}\hat{a}^\dagger_{u\tau}\hat{a}_{j\tau} \quad a\le b, \\
\hat{V}^{(0)}_{i,a} &= \sum_{tu}^{active}\sum_{\sigma\tau}^{-1/2,1/2}\left\{(ia\,|\,tu)\,\hat{a}^\dagger_{a\sigma}\hat{a}_{i\sigma}\hat{a}^\dagger_{t\tau}\hat{a}_{u\tau} + (it\,|\,ua)\,\hat{a}^\dagger_{t\sigma}\hat{a}_{i\sigma}\hat{a}^\dagger_{a\tau}\hat{a}_{u\tau}\right\} + \sum_{\sigma}^{-1/2,1/2} h^{eff}_{ai}\hat{a}^\dagger_{a\sigma}\hat{a}_{i\sigma}, \\
\hat{V}^{(-1)}_{a} &= \sum_{tuv}^{active}\sum_{\sigma\tau}^{-1/2,1/2}\left\{(au\,|\,tv)\,\hat{a}^\dagger_{a\sigma}\hat{a}_{u\sigma}\hat{a}^\dagger_{t\tau}\hat{a}_{v\tau}\right\} + \sum_{t}^{act}\sum_{\sigma}^{-1/2,1/2} h^{eff'}_{at}\hat{a}^\dagger_{a\sigma}\hat{a}_{t\sigma}, \\
\hat{V}^{(1)}_{i} &= \sum_{tuv}^{active}\sum_{\sigma\tau}^{-1/2,1/2}\left\{(iu\,|\,tv)\,\hat{a}^\dagger_{a\sigma}\hat{a}_{u\sigma}\hat{a}^\dagger_{v\tau}\hat{a}_{t\tau}\right\} + \sum_{t}^{act}\sum_{\sigma}^{-1/2,1/2} h^{eff}_{ti}\hat{a}^\dagger_{t\sigma}\hat{a}_{i\sigma},
\end{aligned} \tag{11}$$

with $\gamma_{pq} = 1 - \frac{1}{2}\delta_{pq}$. For perturber classes with contractions over active indices the two-electron (and one-electron) integrals act as weights in the summation and hence account for the specific importance of each contributing function. The effective one-electron integrals h^{eff}_{pq} and $h^{eff'}_{pq}$ in Equation (11) incorporate the interaction between active and internal orbitals in a mean-field way and are defined as

$$\begin{aligned} h^{eff}_{pq} &= h_{pq} + \sum_i 2\,(ii\,|\,pq) - (pi\,|\,iq), \\ h^{eff'}_{pq} &= h^{eff}_{pq} - \sum_t (pt\,|\,tq). \end{aligned} \tag{12}$$

It can be seen that the perturber functions $\left|\Psi_\lambda^{(n_k)}\right\rangle$ in Equation (10) are orthogonal but not normalized.[5] The squared norm $N_\lambda^{(n_k)} = \left\langle\Psi_\lambda^{(n_k)}|\Psi_\lambda^{(n_k)}\right\rangle$ plays an important role for SC-NEVPT2 as it enters the equation for the second order perturbed energy as well as for the first order perturbed wavefunction,

$$\begin{aligned} E^{(2)} &= \sum_{n_k\lambda}\frac{N_\lambda^{(n_k)}}{E_m^{(0)} - E_\lambda^{(n_k)}}, \\ \Psi_m^{(1)} &= \sum_{n_k\lambda}\left|\Psi_\lambda^{(n_k)}\right\rangle\frac{\sqrt{N_\lambda^{(n_k)}}}{E_m^{(0)} - E_\lambda^{(n_k)}}. \end{aligned} \tag{13}$$

A critical aspect of the SC-NEVPT2 method is the assignment of an energy $E_l^{(k)}$ to a given perturber function $\Psi_l^{(k)}$. In many instances of multireference perturbation theory, $E_l^{(k)}$ is taken as the energy expectation value $\left\langle \Psi_\lambda^{(n_k)} \middle| \hat{H} \middle| \Psi_\lambda^{(n_k)} \right\rangle$ and the same choice has been made in this work. The complexity of the computation of $E_l^{(k)}$ is significantly reduced by applying Dyall's approximation to the zeroth order Hamiltonian. Within this approximation the Hamiltonian is divided into an inactive part that only contains diagonal one-electron terms and a more sophisticated active part,[56]

$$\hat{H}_0^{Dyall} = \sum_i \varepsilon_i \hat{E}_i^i + \sum_a \varepsilon_a \hat{E}_a^a + C + \sum_{tu} \hat{h}_{tu}^{eff} \hat{E}_u^t + \frac{1}{2} \sum_{tuvw} (tu \,|\, vw) \left\{ \hat{E}_u^t \hat{E}_w^v - \delta_{uv} \hat{E}_w^t \right\}, \tag{14}$$

with $\hat{E}_q^p = \sum_\sigma^{-1/2,1/2} \hat{a}_{p\sigma}^\dagger \hat{a}_{q\sigma}$ being second quantized replacement operators. The presence of the full two-electron interaction within the active orbital space in $\hat{H}_0^{Dyall}$ ensures the absence of any intruder-state problems in SC-NEVPT2 calculations. Furthermore, $\Psi_m^{(0)}$ is still an eigenfunction of $\hat{H}_0^{Dyall}$ and given the right choice of constant $C = 2\sum_i h_{ii} + \sum_{ij} \{2\,(ii \,|\, jj) - (ij \,|\, ji)\} - 2\sum_i \varepsilon_i$ the eigenvalue of the reference function $\Psi_m^{(0)}$ is unaltered by this choice of zeroth order Hamiltonian. Hence,

$$\hat{H}_0^{Dyall} \left| \Psi_m^{(0)} \right\rangle = E_m \left| \Psi_m^{(0)} \right\rangle. \tag{15}$$

In the following, when $\hat{H}_0$ is used, we imply usage of $\hat{H}_0^{Dyall}$.

In regular SC-NEVPT2 calculations on top of a CASCI or CASSCF reference function, the norm $N_\lambda^{(n_k)}$ and energy expectation value $E_\lambda^{(n_k)}$ of any given perturber function is evaluated using active space densities of up to fourth order of the zeroth order function. The corresponding formulae can be found in the original works of Angeli *et al.*[5,6] Sheng *et al.* implemented this classical approach to incorporating SC-NEVPT2 with DMRG.[33] As outlined above, this approach is in general not feasible for large-scale DMRG calculations with more than 24 orbitals due to the cost of computing the 4-particle density matrix. For this reason, in Sec. II C we will introduce a projection approximation to reduce the cost of evaluating the norm and energy expectation value for the most expensive classes of perturber functions. For perturber classes $\hat{V}_{ij,ab}^{(0)}$, $\hat{V}_{ab,i}^{(-1)}$, and $\hat{V}_{ij,a}^{(1)}$, however, the evaluation of $N_\lambda^{(n_k)}$ and $E_\lambda^{(n_k)}$ requires density matrices of only up to second order. Therefore, these classes are treated in a classical way using density matrices provided by the DMRG calculation.[57,58]

At this point, it needs to be noted that the combination of DMRG and the strongly contracted form of NEVPT2 faces two fundamental problems. First, the error introduced by the contraction over active indices will increase with the size of the active space. The integrals incorporated in the definition of the contracted perturber functions (cf. Equation (11)) act as weights of the different functions in the contraction and partially redeem this shortcoming. Nevertheless, the contraction error will become non-negligible for active spaces on the order of 20-40 orbitals. Second, it has recently been shown by Neese *et al.* that the SC-NEVPT2 method is not invariant with respect to orbital rotations within the active space.[59] Thus, results that have been obtained from a DMRG-SC-NEVPT2 calculation with localized active orbitals may differ from their canonical counterparts.

C. DMRG-proj-SC-NEVPT2

1. Renormalized perturber functions

This section outlines the details of the presented approach to SC-NEVPT2 as a means of treating dynamic electron correlation in a quantum chemical DMRG calculation. First, it should be noted that, if applied as described above, the DMRG algorithm yields an approximation to the FCI solution for the active orbital space that does not contain any reference to the internal orbitals. The connection to the internal orbitals is restored by replacing the one-electron integrals in the Hamiltonian matrix (cf. Equation (7)) by the effective one-electron integrals h_{pq}^{eff} from Equation (12). Furthermore, in order to construct a suitable zeroth order wavefunction the resulting MPS has to be multiplied with an orbital product of doubly occupied internal orbitals,

$$\Psi^{(0)} = \Psi_{MPS} \otimes \Phi^{(0)}. \tag{16}$$

In Equation (16), the index m was dropped because it is implied that Ψ_{MPS} approximates the electronic ground state. In principle, however, the presented formalism is applicable to any excited state as well. The orbital product function $\Phi^{(0)}$ describes a fully occupied set of internal orbitals together with an empty set of virtual orbitals. It should be noted that the procedure illustrated in Equation (16) is completely analogous to the construction of perturber functions in Sec. II B. Based on Equation (16) one could define perturbers by acting the operators in Equation (11) on the zeroth order wavefunction. Because of the special form of the perturber operators, the resulting perturber function would also be in the form of Equation (16), namely a MPS multiplied by a simple orbital product function (now with additional holes and particles outside of the active space). However, the resulting MPS would in general be of larger bond dimension than the bond dimension used for the zeroth order DMRG wavefunction. Further, it would involve a different set of site tensors to the zeroth order wavefunction. Simplifications occur therefore if we project the action of perturber operators into the renormalized states of the DMRG wavefunction associated with a given site w. This ensures that the perturber functions share the same site tensors as the zeroth order wavefunction save for the $\boldsymbol{C}$ tensor at site w. With the projector on the canonical representation of site w being defined as $\hat{P}_w^{DMRG} = \sum_{l'_w r_w} \left| l'_w r_w \right\rangle \left\langle l'_w r_w \right|$ and $\hat{Q}_w^{DMRG} = \hat{P}_w^{DMRG} \otimes \hat{\mathbf{1}}_{inactive}$ we can thus project any (strongly contracted) perturber function in the desired form,

$$\tilde{\Psi}_\lambda^{(n_k)} = \hat{Q}_w^{DMRG} \Psi_\lambda^{(n_k)} = \hat{Q}_w^{DMRG} \hat{V}_\lambda^{(n_k)} \left| \Psi^{(0)} \right\rangle. \tag{17}$$

Accordingly, the second order perturbed energy becomes

$$E^{(2)} = \sum_{kl} \frac{N_\lambda^{(n_k)}}{E_m^{(0)} - E_\lambda^{(n_k)}} = \sum_{kl} \frac{\langle \Psi^{(0)} | \hat{V}_\lambda^{(n_k)\dagger} \hat{Q}_w^{DMRG} \hat{V}_\lambda^{(n_k)} | \Psi^{(0)} \rangle}{E^{(0)} - \langle \Psi^{(0)} | \hat{V}_\lambda^{(n_k)\dagger} \hat{Q}_w^{DMRG} \hat{H}_0 \hat{Q}_w^{DMRG} \hat{V}_\lambda^{(n_k)} | \Psi^{(0)} \rangle}. \quad (18)$$

As the presented method currently only calculates perturbed energies, Equation (18) is the central equation of this work. Note that Equation (18) gives the exact SC-NEVPT2 energy in the limit of an infinitely large bond dimension. For finite bond dimension, the projection approximation will be most accurate if we choose a site w near the middle of the lattice, since it is here that the largest number of renormalized states appear. For this reason, we will work with the projection to the renormalized states at the middle of the lattice denoted by $w = \bar{t}$.

2. Calculation of the norm and the energy expectation value

In order to evaluate the norm and energy expectation values in Equation (18) the perturber functions $\tilde{\Psi}_\lambda^{(n_k)}$ need to be constructed in the renormalized space of the DMRG algorithm. Creation and annihilation operators that act on the inactive orbital space do not have to be evaluated explicitly since the inactive part of the zeroth order function takes a very simple form and the unperturbed Hamiltonian $\hat{H}_0$ as well as the projection operator $\hat{Q}_w^{DMRG}$ feature only diagonal elements. In contrast, the active part of the perturber functions is constructed explicitly using the reduced one- and two-index renormalized operator matrices (*vide supra*) available from the preceding DMRG calculation.[10,55] For example, the perturber function $\tilde{\Psi}_{ab}^{(-2)}$ is constructed in the renormalized DMRG basis according to

$$\langle l'_w r_w \otimes ab; SM | \hat{V}_{ab}^{(-2)} | \Psi^{(0)} SM \rangle = \sum_{S'=S-1}^{S+1} \sum_{\Gamma=0}^{1} \sum_{tu} \frac{\sqrt{2S'+1}}{\sqrt{2S+1}} \langle l'_w r_w S' \| \hat{A}_{tu}^{\dagger\Gamma} \| \Psi_{MPS} S \rangle \cdot (au|bt) \cdot \sum_{M'=-S'}^{S'} \sum_{m=-\Gamma}^{\Gamma} (-1)^{\Gamma+m} \times U_{SM}^{\Gamma-mS'M'} U_{SM}^{\Gamma-mS'M'}. \quad (19)$$

The term $|ab\rangle$ on the left hand side of Equation (19) represents an orbital product of inactive orbitals with additional electrons in external orbitals a and b whereas $|l'_w r_w\rangle$ denotes a function contained in the renormalized active space. Moreover, the pairs of numbers (S,M), (S',M'), and (Γ,m) denote total spin and magnetic spin quantum numbers. The last term on the right hand side of Equation (19) features a sum of Clebsch-Gordan coefficients which for $S = 0$ becomes $\sum_{M'=-S'}^{S'} \sum_{m=-\Gamma}^{\Gamma} (-1)^{\Gamma+m} U_{00}^{\Gamma-mS'M'} U_{00}^{\Gamma-mS'M'} = \delta_{S'\Gamma}$. Analogous formulas to Equation (19) for $\tilde{\Psi}_{ij}^{(2)}$ and $\tilde{\Psi}_{ia}^{(0)}$ can be found in Appendix A.

Once the perturber functions are constructed in a given renormalized representation their norm is readily calculated as a vector product in the renormalized basis $\{|l'_w r_w\rangle\}$. As all inactive operators only contribute terms of the form $\delta_{aa}\delta_{bb} = 1$ to the norm the inactive part of the perturber function enters the norm only indirectly via the one- and two-electron integrals. Analogous to the norm, the energy expectation value of a given perturber function is evaluated as a vector times matrix times vector product in the same renormalized basis as the norm. The required multiplication of a function with the superblock Hamiltonian matrix is carried out efficiently as described elsewhere.[10] Here, the inactive part contributes with an orbital energy difference. For example,

$$\langle \Psi_{ia}^{(0)} | \hat{H}_0 | \Psi_{ia}^{(0)} \rangle = \mathbf{\Psi}_{ia}^{(0)T} \boldsymbol{H}_0 \mathbf{\Psi}_{ia}^{(0)} + \varepsilon_i - \varepsilon_a, \quad (20)$$

where the first term on the right hand side denotes the vector times matrix times vector multiplication in the renormalized active space and ε_a and ε_i refer to the orbital energies of orbitals a and i, respectively.

3. Construction and accumulation of three-index operators

The construction of perturber functions $\tilde{\Psi}_a^{(-1)}$ and $\tilde{\Psi}_i^{(1)}$ in the renormalized basis of a site $\bar{t} = \frac{k}{2}$ necessitates the generation of operators with three active indices that are not available from the preceding DMRG calculation (cf. Equation (11)). Of course, it is highly desirable to construct them as a product of local operators as outlined in Equation (8). The actual form of such a product of operators depends on the distribution of the three active indices t, u, and v over two blocks. If the indices are not all located on the same block, there exist three possible distributions, each corresponding to a different product of operators. For example, the following expressions are obtained for the reduced three-index operator matrix $\hat{\boldsymbol{O}}_{tuv}^{1/2}$ that appears in $\tilde{\Psi}_a^{(-1)}$:

Case 1: t and u are on the same block

$$\hat{\boldsymbol{O}}_{tuv}^{1/2} = \sqrt{2} \hat{\boldsymbol{E}}_{tu}^{0} \otimes_{1/2} \hat{\boldsymbol{a}}_v^{1/2}. \quad (21)$$

Case 2: t and v are on the same block

$$\hat{\boldsymbol{O}}_{tuv}^{1/2} = \sum_{\Gamma=0}^{1} \frac{\sqrt{2\Gamma+1}}{\sqrt{2}} \hat{\boldsymbol{E}}_{tv}^{\Gamma} \otimes_{1/2} \hat{\boldsymbol{a}}_u^{1/2}. \quad (22)$$

Case 3: u and v are on the same block

$$\hat{\boldsymbol{O}}_{tuv}^{1/2} = \sum_{\Gamma=0}^{1} (-1)^{\Gamma} \frac{\sqrt{2\Gamma+1}}{\sqrt{2}} \hat{\boldsymbol{A}}_{tv}^{\Gamma} \otimes_{1/2} \hat{\boldsymbol{a}}_u^{1/2}. \quad (23)$$

Analogous formulas for the operator appearing in $\tilde{\Psi}_i^{(1)}$ are given in Appendix B. It is important to note that the distribution of a given set of indices over two blocks depends on the position in the sweep one is in. Consequently it is possible to express the great majority of terms required for the construction of $\tilde{\Psi}_a^{(-1)}$ and $\tilde{\Psi}_i^{(1)}$ as a product of local operators. One must only choose an adequate iteration in the sweep for each term (*vide infra*) and then apply subsequent renormalizations to obtain the appropriate (and now approximate) representation for site $\bar{t}$. The very few exceptions are only met when $t = u = v$. In these cases Equation (21) is also used but the tensor product cannot be taken as a product of local tensors but has to be carried out

explicitly in the local basis $\{|n_t\rangle\}$. But since the Hilbert space on a single site is only 4-dimensional this is feasible.

In order to evaluate as many three index-operators as possible as a product of two local operators according to Equations (21)–(23) the operator matrices are generated and accumulated over the course of two sweeps, in the following referred to as forward and backward sweep. During each iteration of the forward sweep all three-index operator matrices with at least one index located on the dot-block and the remaining indices located on the left block are constructed until the middle of the lattice is reached. In this way, every operator matrix with three indices on the left half of the lattice is constructed once (and only once!). At the beginning of a given iteration all previously constructed matrices are brought to the current canonical representation according to

$$\hat{\boldsymbol{O}}^{new}_{tuv} = \hat{\boldsymbol{O}}^{old}_{tuv} \otimes \hat{\mathbf{1}}_{n_t}, \tag{24}$$

where t is the site that corresponds to the dot-block $\bullet$. At the end of the renormalization step all constructed three-index operator matrices are renormalized using the left rotation matrix $\boldsymbol{L}_{n_i}$,

$$\hat{\boldsymbol{O}}^{new}_{tuv} = \boldsymbol{L}^T_{n_t} \hat{\boldsymbol{O}}^{old}_{tuv} \boldsymbol{L}_{n_t}. \tag{25}$$

When the middle of the lattice is reached, all three-index operators that are entirely located on the left side of the lattice are constructed and brought to the canonical representation associated with site $\bar{t} = \frac{k}{2}$. During the remaining iterations of the forward sweep the constructed three-index operator matrices are left untouched and no further matrices are constructed. All matrices with indices exclusively on the right hand side of the lattice are constructed and transformed in the same fashion during the first half of the backward sweep. Eventually, when the backward sweep reaches the middle of the lattice two sets of operators with their indices located exclusively on the left and right side of the lattice, respectively, are available in the canonical representation associated with site $\bar{t}$. The remaining operators are readily evaluated as product of local operators in $\left\{\left|l'_{\bar{t}}\right\rangle\right\}$ and $\{|r_{\bar{t}}\rangle\}$. With all required three-index operator matrices at hand the perturber function $\tilde{\Psi}^{(-1)}_a$ is formed as

$$\begin{aligned}
&\left\langle l'_{\bar{t}} r_{\bar{t}} \otimes a; SM \middle| V^{(-1)}_a \middle| \Psi^{(0)} SM \right\rangle \\
&\quad = \sum_t \sum_{S'=|S-1/2|}^{S+1/2} \frac{\sqrt{2S'+1}}{\sqrt{2S+1}} h^{eff}_{at} \left\langle l'_{\bar{t}} r_{\bar{t}} S' \middle\| \hat{a}^{1/2}_t \middle\| \Psi S \right\rangle \\
&\qquad + \sum_{tuv} \sum_{S'=|S-1/2|}^{S+1/2} \frac{\sqrt{2S'+1}}{\sqrt{2S+1}} \\
&\qquad \times \left\langle l'_{\bar{t}} r_{\bar{t}} S' \middle\| \hat{O}^{1/2}_{tuv} \middle\| \Psi S \right\rangle \cdot (av \,|\, \boldsymbol{tu}) .
\end{aligned} \tag{26}$$

The corresponding formula for $\tilde{\Psi}^{(1)}_i$ is given in Appendix B.

4. A modified renormalization scheme

Projection of the perturber function on the renormalized active space of site $\bar{t}$ as outlined in Section II C 1 implies that some information about the perturber functions is discarded unless, of course, the bond dimension is infinite. Thus only if the discarded information is not essential for the correct evaluation of the norm and energy expectation value are the here made approximations valid. However, in the regular DMRG algorithm the renormalized space is optimized to yield the best possible $4M^2$-dimensional representation of the electronic ground state, which does not coincide with the optimal representation of the perturber functions. A more suitable representation of the perturber functions can be obtained by taking them into account explicitly during the renormalization step. In the presented method, the modified density matrix

$$\rho' = \alpha \left|\Psi_{MPS}\right\rangle \left\langle\Psi_{MPS}\right| + (1-\alpha)\, \rho^{perturber} \tag{27}$$

enters the SVD. This modified density is a weighted sum of the electronic ground state density and the active part of the density of the first order interacting space (FOIS). More precisely,

$$\begin{aligned}
\hat{\rho}^{perturber} = &\sum_t w_t(S,S') \left|\Psi^t SS'\right\rangle \left\langle\Psi^t SS'\right| \\
&+ \sum_u w_u(S,S') \left|\Psi_u SS'\right\rangle \left\langle\Psi_u SS'\right| \\
&+ \sum_{tu} \sum_{\Gamma} w_{tu}(S,S',\Gamma) \left|\Psi^t_u SS'\Gamma\right\rangle \left\langle\Psi^t_u SS'\Gamma\right| \\
&+ \sum_{tu} \sum_{\Gamma} w'_{tu}(S,S',\Gamma) \left|\Psi^t_u SS'\Gamma\right\rangle \left\langle\Psi^t_u SS'\Gamma\right| \\
&+ \sum_{tu} \sum_{\Gamma} w''_{tu}(S,S',\Gamma) \left|\Psi_{tu} SS'\Gamma\right\rangle \left\langle\Psi_{tu} SS'\Gamma\right| \\
&+ \sum_{tuv} w_{tuv}(S,S') \left|\Psi^{tu}_v SS'\right\rangle \left\langle\Psi^{tu}_v SS'\right| \\
&+ \sum_{tuv} w'_{tuv}(S,S') \left|\Psi^t_{uv} SS'\right\rangle \left\langle\Psi^t_{uv} SS'\right|
\end{aligned} \tag{28}$$

which is a weighted sum of densities that correspond to wavefunctions that originate from the action of active space creation and annihilation operators on the ground state MPS, such as $\left|\Psi^t_u SS'\Gamma\right\rangle = \left(\hat{a}^\dagger_t \hat{a}_u\right)^\Gamma \otimes_{S'} \left|\Psi_{MPS} S\right\rangle$. The weights in Equation (28) are defined as the sum of squares of the products of electronic integrals and prefactors as they appear in the definition of the corresponding perturber classes (c.f., for example, Equation (19)). For example,

$$w_{tu}(S,S',\Gamma) = \sum_{ij} \left(\frac{\sqrt{2S'+1}}{\sqrt{2S+1}} \cdot (tj \,|\, ui) \cdot \sum_{M'=-S'}^{S'} \sum_{m=-\Gamma}^{\Gamma} (-1)^{\Gamma+m} U^{\Gamma-m S'M'}_{SM} U^{\Gamma-m S'M'}_{SM} \right)^2 . \tag{29}$$

Introducing the density of Equation (27) to the renormalization procedure ensures that those parts of the active space that are most important for the description of the perturber functions are incorporated in the renormalized space. Of course, this improvement comes at the cost of a slightly slower convergence of the ground state energy with respect to the bond dimension M as compared to the standard renormalization procedure. However, this effect is negligible in reality because the convergence of the perturbation energy is much slower than the convergence of the ground state energy. Eventually it is important to note that the actual value of the reference density weight α does not alter the final result as one should converge both the ground state and the perturbation energy up to a given threshold. Accordingly, α only influences the relative convergence rate of both quantities. If not otherwise stated, all calculations in Sec. III apply the here presented renormalization scheme.

5. Scaling

The scaling of computational time and memory requirements with respect to increasing the size of the orbital spaces (n_{int}, $n_{act} = k$ and n_{ext}) and the bond dimension M is a critical aspect of any quantum chemical DMRG calculation. Table I summarizes the scaling of time and memory requirements for the five classes of perturber functions that are evaluated non-classically. In the case of $\tilde{\Psi}^{(-2)}_{ab}$, $\tilde{\Psi}^{(2)}_{ij}$, and $\tilde{\Psi}^{(0)}_{ia}$ the CPU time scaling depends on three steps of the calculation. The first step involves the generation of the two-index operators and their contraction with Ψ_{MPS} and scales as $O\left(n^2_{act}M^3\right)$. After their formation the intermediates of the form $\boldsymbol{V}_{tu} = \boldsymbol{O}_{tu}\boldsymbol{C}$ are kept in memory requiring memory that scales as $O\left(n^2_{act}M^2\right)$. Each of the n^2_{act} intermediates is then contracted with the electronic Hamiltonian taking $O\left(n^4_{act}M^3\right)$ CPU time and results in intermediates $\boldsymbol{\sigma}_{tu} = \boldsymbol{H}_0\boldsymbol{V}_{tu}$ with storage requirements of $O\left(n^2_{act}M^2\right)$. Eventually, the perturber functions are built from the prestored intermediates with a cost of $O\left(n^2_{ext}n^2_{act}M^2\right)$ for $\tilde{\Psi}^{(-2)}_{ab}$. Note that for $\tilde{\Psi}^{(2)}_{ij}$ and $\tilde{\Psi}^{(0)}_{ia}$ the cost for this step actually scales as $O\left(n^2_{int}n^2_{act}M^2\right)$ and $O\left(n_{ext}n_{int}n^2_{act}M^2\right)$, respectively. However, since generally the number of external orbitals, n_{ext}, exceeds the number of internal orbitals, n_{int}, the step of $O\left(n^2_{ext}n^2_{act}M^2\right)$ will become the computational bottleneck. Generally, the memory requirements on the order of $O\left(n^2_{act}M^2\right)$ are of the same order of magnitude as those of the underlying DMRG calculation.

The calculation of the contributions from $\tilde{\Psi}^{(-1)}_{a}$ and $\tilde{\Psi}^{(1)}_{i}$ features five significant steps starting with the generation of the operator matrices whose indices are located only on one side of the lattice (*vide supra*). This step scales as $O\left(n^3_{act}M^2\right)$ in computational time and since the storage requirement scales as $O\left(n^3_{act}M^2\right)$ the operator matrices are stored on disk. However, it is noteworthy that since the index combinations for these operators are strongly restricted the requirement is reduced by a factor of $\left(\frac{1}{2}\right)^3 = \frac{1}{8}$. As outlined above, the three-index operators need to be renormalized during the modified sweeps with a computational cost that scales as $O\left(n^3_{act}M^3\right)$. The third step involves the contraction of all three-index operators with Ψ_{MPS} which costs $O\left(n^3_{act}M^3\right)$ computational time. Importantly, the resulting intermediates $\boldsymbol{V}_{tuv} = \boldsymbol{O}_{tuv}\boldsymbol{C}$ are not kept in memory but directly added to the final perturber functions thus prohibiting a true storage requirement of $O\left(n^3_{act}M^2\right)$. Generating the perturber functions in this way scales as $O\left(n^3_{act}n_{ext/int}M^2\right)$ and requires $O\left(n_{ext/int}M^2\right)$ memory. In the last step the active Hamiltonian is contracted with $\tilde{\Psi}^{(1)}_{i}$ and $\tilde{\Psi}^{(1)}_{i}$ which scales as $O\left(n^2_{act}n_{ext/int}M^3\right)$. For the evaluation of contributions from $\tilde{\Psi}^{(-1)}_{a}$ and $\tilde{\Psi}^{(1)}_{i}$ this step together with the renormalization and contraction of the three-index operators constitutes the computational bottleneck. At this point it should be noted that each renormalization step as it is introduced in Sec. II C 4 requires contraction of some one-, two-, and three-index operators with Ψ_{MPS}. Hence, the computational time for each renormalization step scales as $3 \cdot \tilde{n}^2_{act}M^3 + 2 \cdot \tilde{n}^3_{act}M^3$ where $\tilde{n}_{act}$ denotes the number of sites on the left (or right) block. However, the second, larger term only applies until the middle of the lattice is reached. The generation of the weights from Equation (28) scales as $n^2_{ext}\tilde{n}^2_{act} + n_{ext}n_{int}\tilde{n}^2_{act} + n^2_{int}\tilde{n}^2_{act} + n_{ext}\tilde{n}^3_{act} + n_{int}\tilde{n}^3_{act}$ which is usually negligible compared to the cost of the contraction.

Note that in the projected implementation, the choice has been made for each perturber class to minimize the scaling with respect to the number of active orbitals, even at a cost of quadratic scaling with the number of external orbitals. However, it is possible to mix and match the projected treatment of one class of perturber functions with a classical treatment of other classes. For example, if one chooses to build the 3-particle density matrix in a classical sense,[33] the dominant scaling to treat the $\Psi^{(-2)}_{ab}$ and $\Psi^{(2)}_{ij}$ perturbers becomes $M^3n^4_{act} + M^2n^6_{act}$, eliminating the main dependence on the number of external functions. We can also compare the overall scaling of the projected algorithm with the scaling of the classical treatment of all perturbers. There, the main cost comes from perturber classes $\Psi^{(-1)}_{a}$ and $\Psi^{(1)}_{i}$, which involve the construction of the 4-particle active space density matrix, leading to a scaling of $M^3n^5_{act} + M^2n^8_{act}$. If we assume $n_{ext} \propto n_{act}$, then we see that the projection approximation significantly lowers the scaling of the SC-NEVPT2 algorithm

TABLE I. Scalings of computational costs and memory requirement for different perturber classes.

Perturber class	CPU time scaling	Memory scaling
$\Psi^{(-2)}_{ab}$	$n^2_{act}M^3 + n^4_{act}M^3 + n^2_{act}n^2_{ext}M^2$	$n^2_{act}M^2 + n^2_{act}M^2$
$\Psi^{(2)}_{ij}$	$n^2_{act}M^3 + n^4_{act}M^3 + n^2_{act}n^2_{int}M^2$	$n^2_{act}M^2 + n^2_{act}M^2$
$\Psi^{(0)}_{ia}$	$n^2_{act}M^3 + n^4_{act}M^3 + n^2_{act}n_{ext}n_{int}M^2$	$n^2_{act}M^2 + n^2_{act}M^2$
$\Psi^{(-1)}_{a}$	$n^3_{act}M^2 + n^3_{act}M^3 + n^3_{act}M^3 + n^3_{act}n_{ext}M^2 + n^2_{act}n_{ext}M^3$	$n^3_{act}M^2 + n_{ext}M^2$
$\Psi^{(1)}_{i}$	$n^3_{act}M^2 + n^3_{act}M^3 + n^3_{act}M^3 + n^3_{act}n_{int}M^2 + n^2_{act}n_{int}M^3$	$n^3_{act}M^2 + n_{int}M^2$

as compared to the classical implementation, thus potentially allowing very large active spaces to be treated. The price to pay is a projection error which must be converged with the bond dimension. The numerical consequences of this error we will now examine in Sec. III.

III. RESULTS

A. The N_2 molecule

In this section a number of test calculations on the N_2 molecule are presented and discussed in order to demonstrate some key features of the projected DMRG-SC-NEVPT2 method. All presented calculations were performed using a fully parallel version of the BLOCK program and feature an active space of 8 electrons in 10 orbitals.[10,55] The active and inactive orbitals were optimized in a preceding CASSCF calculation that employed the def2-TZVP basis set using the ORCA program package.[60,61] Note that during the calculations presented in this section a feature of the BLOCK program that automatically discards all states with an eigenvalue of less than 10^{-12} in the SVD was disabled.

First, the impact of the modified renormalization scheme described in Section II C 4 on projected DMRG-SC-NEVPT2 calculations was investigated. Figure 2 depicts the total energy of N_2 at a bond distance of 1.1 Å with respect to the bond dimension M in the range of $M = 30 - 150$ states for a varying reference density weight α. All observed changes in the total energy in Figure 2 solely originate from changes of the perturbation energy since the unperturbed energy is already converged to within 1 mE_h of the CASCI value for $M = 25$. When the FOIS density is not considered during renormalization ($\alpha = 1$) the energy decreases steeply and converges to within 0.1 mE_h of the exact CASCI+SC-NEVPT2 value for $M = 125$. The curve for $\alpha = 0.5$ in Figure 2 nicely demonstrates that the convergence of the total energy towards the exact value is substantially accelerated by taking the FOIS density into account according to Equation (27). Shifting the reference density weight to $\alpha = 0.3$ and $\alpha = 0.7$ leads to only small energy differences compared to $\alpha = 0.5$ (in fact the results for $\alpha = 0.7$ and $\alpha = 0.5$ are virtually indistinguishable in Figure 2). However, when only the FOIS density enters the SVD ($\alpha = 0$) the total energy starts at a considerably lower value but converges much slower ($M = 500$, not shown in Figure 2) to the final value than for $\alpha = 0.5$. Interestingly, the total energy approaches the exact value from below in this case. In summary, the presented results demonstrate that only an even mixture of reference and FOIS density yields the desired convergence behavior.

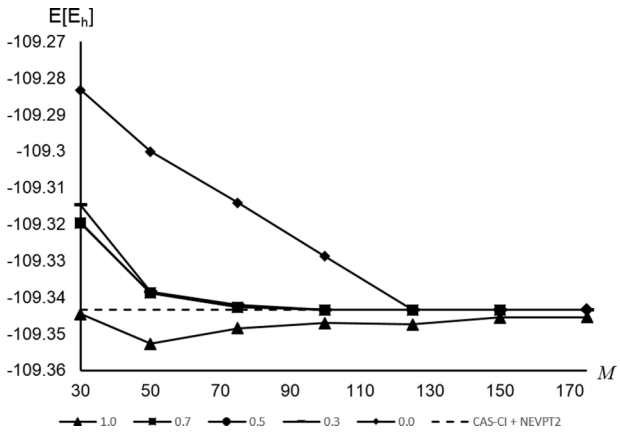

FIG. 2. Total energy of N_2 calculated with projected DMRG-NEVPT2 for varying bond dimensions and reference density weights.

The importance of converging the total energy is underlined by the results presented in Figures 3(a) and 3(b). It shows the calculated binding curve of N_2 with varying bond dimension M in comparison to the results obtained from regular SC-NEVPT2 theory (denoted as CASCI+SC-NEVPT2 results). For bond dimensions of $M = 30$ and $M = 50$ the binding curve exhibits several visible bumps that correspond to an unphysical behavior. The data presented in Figure 3(b) reveal that the deviation from the exact curve appears to be arbitrary (but positive) and does not follow a systematic pattern. Only a tendency to higher deviations for larger bond distances can be observed which may originate from the more complicated structure of the wavefunction in the bond breaking scenario. The lack of systematic errors with different bond lengths reflects the fact that the DMRG sweeps at different bond lengths may choose to retain renormalized states of slightly different character (e.g., with a different distribution of quantum numbers). At the M values considered here, this behavior leads to only very small non-smoothness of the CAS-CI energy, which is well converged at modest M, but leads to large jumps in the PT2 energy, which requires larger bond dimensions to converge. In principle, to ensure smoothness one can use maximum overlap methods to adiabatically evolve the DMRG renormalized basis from one geometry to the next, but this was not done here. As expected, with increasing bond dimension the deviations decrease and the calculated binding curves approach the exact CASCI+SC-NEVPT2 curve. At a value of $M = 100$ the curve in Figure 3(a) is virtually indistinguishable from the exact curve and the deviation is on the order of a few mE_h (<5 mE_h, cf. Figure 3(b)). When M is increased further, the error decreases below the mE_h level. Similar observations are made for the calculated spectroscopic constants displayed in Table II. For a bond dimension of $M = 100$, when smoothness of the binding curve is ensured, the calculated harmonic frequency ω_e approaches the frequency obtained for the combination of CASCI+SC-NEVPT2. Interestingly, the equilibrium distance R_e and the anharmonicity constant $\omega_e x_e$ are already for $M = 30$ in good agreement with the values obtained from CASCI-+SC-NEVPT2 and MRCI. However, it is somewhat disappointing that M needs to be significantly larger than the M required for an accurate zeroth order wavefunction. This reflects the fact that a single renormalized basis is being used to represent the ground state and the perturbers. This is the price to pay for the low computational scaling with the number of active orbitals of the current algorithm.

B. $[Cu_2O_2(en)_2]^{2+}$

In addition to the rather simplistic calculations on the N_2 molecule we performed more challenging calculations on the

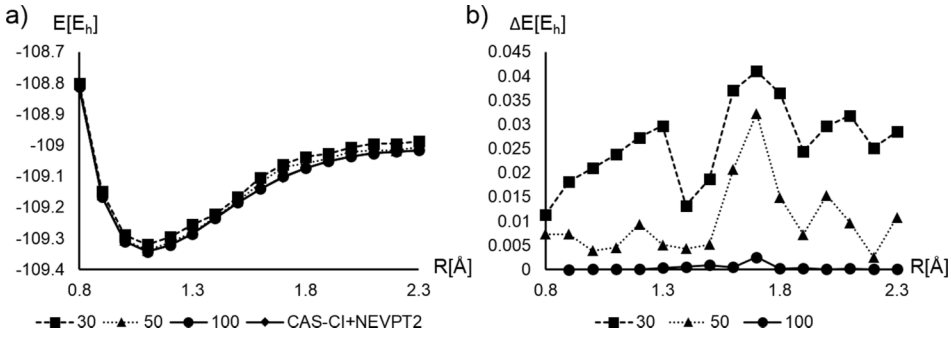

FIG. 3. Calculated binding curves of N_2 (a) and deviation from the exact CASCI+NEVPT2 curve (b) with varying bond dimension M. The reference density weight has been fixed at $\alpha = 0.5$.

TABLE II. Calculated spectroscopic constants for N_2.

	R_e (Å)	ω_e (cm^{-1})	$\omega_e x_e$ (cm^{-1})
CASCI(8,10)/SC-NEVPT2	1.096	2346.7	17.2
DMRG-proj-SC-NEVPT2(M = 30)	1.093	2367.0	17.1
DMRG-proj-SC-NEVPT2(M = 50)	1.091	2395.0	17.7
DMRG-proj-SC-NEVPT2(M = 100)	1.096	2351.2	17.3
MRCI(6,6)	1.093	2366.7	17.9
Experiment[62]	1.097	2358.6	14.3

dimeric $[Cu_2O_2(en)_2]^{2+}$ (Figure 4(a), en = ethylenediamine) complex. $[Cu_2O_2(en)_2]^{2+}$ contains a (Cu_2O_2) core that is an integral feature of the active site in a number of copper enzymes.[63,64] On account of its biological importance, this (Cu_2O_2) core has been subject to a vast number of spectroscopic and theoretical investigations including *ab initio* DMRG calculations.[36,39,65–74] In the course of this work, a series of projected DMRG-SC-NEVPT2 calculations were conducted on "structure 7" from Ref. 74 that features an O–O bond distance of 1.60 Å. All calculations employed an active space of 18 electrons in 20 orbitals that were optimized in a preceding DMRGSCF (M = 1000) calculation with the def2-SVP basis set using the ORCA program package.[60,61] For test and demonstration purposes we chose the active space to be still feasible with the presented method with large bond dimensions but too large for a conventional CASSCF/SC-NEVPT2 treatment. Active orbital occupation numbers close to 0 and 2 indicate that all static electron correlation effects are covered with this active space. Thus, increasing the active space would only serve to include a minor part of the dynamical electron correlation in the underlying DMRG calculation.

Figure 4(b) shows the calculated total energy using the modified renormalization scheme described in Section II C 4 with a fixed reference density weight of $\alpha = 0.5$ versus the used bond dimension. With increasing bond dimension the energy decreases and reaches a value of −3087.1646 E_h at M = 2500. Calculations that employ the "exact" DMRG-SC-NEVPT2 scheme of Guo *et al.* on the same system using the same orbitals yielded a value of 3087.1652 E_h (Figure 4(b)).[33] Due to computational limitations the exact calculations are restricted to bond dimensions of up to M = 1500. However, the exact results are already converged beyond 1 mE_h accuracy at M = 500. These results demonstrate two key features of proj-DMRG-SC-NEVPT2: While the algorithm allows for calculations with larger bond dimensions and has a much lower scaling with active space dimension than exact DMRG-SC-NEVPT2 calculations it unfortunately requires comparably large bond dimensions to achieve the same target accuracy of less than 1 mE_h.

IV. CONCLUSIONS

This work introduces a projected approach to SC-NEVPT2 as a means to describe dynamic electron correlation on top of molecular *ab initio* DMRG calculations. In this approach the contributions to the perturbation energy are calculated in two different ways. The contribution from perturber classes $\Psi^{(0)}_{ij,ab}$, $\Psi^{(-1)}_{i,ab}$, and $\Psi^{(1)}_{ij,a}$ is evaluated according to the formulae given by Angeli *et al.* in their original work using active space reduced density matrices of first and second order.[6] The required reduced density matrices are generated by well established procedures.[57,58] In contrast, the remaining perturber functions are approximated from the one- and two-index renormalized operator matrices that are generated and stored during the underlying DMRG calculation. Formally the latter procedure corresponds to a projection of the perturber functions on the renormalized DMRG space at the centre of the lattice. With the renormalized perturber functions at hand their contribution to the perturbation energy is readily obtained from Equation (18). While for $\tilde{\Psi}^{(-2)}_{ab}$, $\tilde{\Psi}^{(0)}_{i,a}$, and $\tilde{\Psi}^{(2)}_{ij}$ the perturber functions are

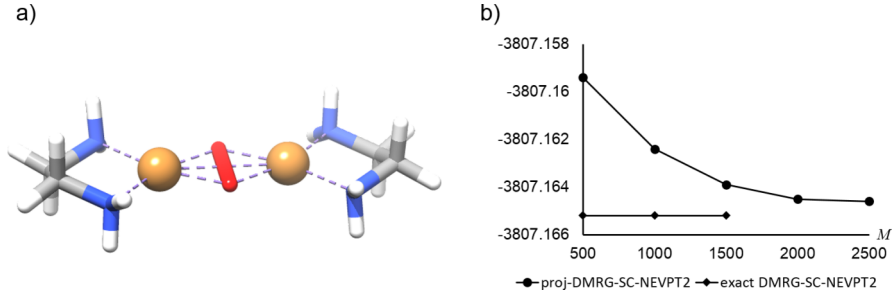

FIG. 4. Ball and stick visualization of $[Cu_2O_2(en)_2]^{2+}$ (a) and total energy calculated with the projected DMRG-NEVPT2 with respect to the bond dimension M (b). The reference density weight in (b) has been fixed to $\alpha = 0.5$.

constructed during a single iteration, the required operator matrices for perturber classes $\tilde{\Psi}_a^{(-1)}$ and $\tilde{\Psi}_i^{(1)}$ are accumulated in the course of two entire sweeps.

The main objective of the presented method is to circumvent the calculation of higher than second order density matrices which becomes prohibitive for large active spaces. Instead, only intermediates with a maximum of three active space indices are generated and stored. This simplification leads to an implementation with a scaling with the number of active orbitals of only n_{act}^4 (assuming the number of external orbitals is proportional to the number of active orbitals). The cost is a loss of accuracy due to the projection approximation. However, as the presented algorithm converges to the exact CASCI+SC-NEVPT2 result for infinite bond dimensions, the accuracy can in principle be estimated and controlled by conducting a series of calculations with varying bond dimension. The convergence of the total energy towards the exact result can be accelerated by using the presented improved renormalization scheme. This takes the action of the perturbing operator explicitly into account and thus yields a more balanced renormalized space.

Test calculations on the N_2 molecule demonstrate the effectiveness of the modified renormalization scheme in improving the renormalized space for the description of the perturber functions and hence the perturbed energy. Still it is somewhat disappointing that converging the perturbation energy to an accuracy of 1 mE_h requires a bond dimension that is significantly larger than the bond dimension required to converge the underlying DMRG CAS calculation to the same accuracy. Furthermore, the potential energy curves shown in Figure 3 emphasize the importance of converging the obtained results with respect to the bond dimension. Otherwise the obtained curves may exhibit jumps. A series of calculations on the dimeric $[Cu_2O_2(en)_2]^{2+}$ indicate that the projection approximation can practically be applied to a complicated problem in a non-trivial active space. However, the most promising route forward for the future may be to sacrifice some of the constraints used in the projection approximation associated with the formally low scaling. For example, different classes of perturbers could use different MPS representations (to achieve higher accuracy for small bond dimensions) and perturbers involving two external indices could be evaluated classically (to remove the large prefactor associated with the ratio of the number of external to active orbitals). Such hybrid algorithmic formulations will be studied in future works.

ACKNOWLEDGMENTS

This work has been funded by the Otto-Hahn award program of the Max-Planck society as well as the US National Science Foundation through Award No. CHE-1265277. Furthermore, M.R. gratefully acknowledges a Research Fellowship of the "Deutsche Akademischer Austausch-Dienst" (DAAD).

APPENDIX A: FORMULAS FOR $\tilde{\Psi}_{ij}^{(2)}$ AND $\tilde{\Psi}_{ia}^{(0)}$

The projection of $\Psi_{ij}^{(2)}$ onto the renormalized space is given by

$$\begin{aligned}\left\langle L_i r_i \otimes ij; SM \middle| \hat{V}_{ij}^{(-2)} \middle| \Psi^{(0)} SM \right\rangle &= \sum_{S'=|S-1|}^{S+1} \sum_{\Gamma=0}^{1} \sum_{tu} \frac{\sqrt{2S'+1}}{\sqrt{2S+1}} \\ &\times \langle L_i r_i S' \| \hat{A}_{tu}^{\Gamma} \| \Psi_{MPS} S \rangle \cdot (tj \,|\, ui) \\ &\cdot \sum_{M'=-S'}^{S'} \sum_{m=-\Gamma}^{\Gamma} (-1)^{\Gamma+m} U_{SM}^{\Gamma-mS'M'} U_{SM}^{\Gamma-mS'M'}, \end{aligned} \tag{A1}$$

whereas the projection of $\Psi_{ia}^{(0)}$ reads to

$$\begin{aligned}\left\langle L_i r_i \otimes ia; SM \middle| \hat{V}_{ab}^{(-2)} \middle| \Psi^{(0)} SM \right\rangle &= 2 \sum_{tu} \langle L_i r_i S \| \hat{E}_{tu}^{0} \| \Psi_{MPS} S \rangle \, (ai \,|\, tu) - \sum_{S'=|S-1|}^{S+1} \sum_{\Gamma=0}^{1} \sum_{tu} \frac{\sqrt{2S'+1}}{\sqrt{2S+1}} \\ &\times \langle L_i r_i S' \| \hat{E}_{tu}^{\Gamma} \| \Psi_{MPS} S \rangle \cdot (au \,|\, ti) \cdot \sum_{M'=-S'}^{S'} \sum_{m=-\Gamma}^{\Gamma} (-1)^{\Gamma+m} U_{SM}^{\Gamma-mS'M'} U_{SM}^{\Gamma-mS'M'}. \end{aligned} \tag{A2}$$

APPENDIX B: FORMULAS FOR $\tilde{\Psi}_i^{(1)}$

The three-index operators appearing in $\tilde{\Psi}_i^{(1)}$ are evaluated according to

Case 1: t and u are on the same block

$$\tilde{\boldsymbol{O}}_{tuv}^{1/2} = \sum_{\Gamma=0}^{1} (-1)^{\Gamma} \frac{\sqrt{2\Gamma+1}}{\sqrt{2}} \hat{\boldsymbol{A}}_{tu}^{\Gamma} \otimes_{1/2} \hat{\boldsymbol{a}}_{v}^{1/2}. \tag{B1}$$

Case 2: t and v are on the same block

$$\tilde{\boldsymbol{O}}_{tuv}^{1/2} = \sum_{\Gamma=0}^{1} (-1)^{1+\Gamma} \frac{\sqrt{2\Gamma+1}}{\sqrt{2}} \hat{\boldsymbol{E}}_{tv}^{\Gamma} \otimes_{1/2} \hat{\boldsymbol{a}}_{u}^{\dagger 1/2}. \tag{B2}$$

Case 3: u and v are on the same block

$$\tilde{\boldsymbol{O}}_{tuv}^{1/2} = \sqrt{2} \hat{\boldsymbol{E}}_{uv}^{0} \otimes_{1/2} \hat{\boldsymbol{a}}_{t}^{\dagger 1/2}. \tag{B3}$$

With these expressions at hand the perturber function $\tilde{\Psi}_i^{(1)}$ is constructed using

$$\begin{aligned}\left\langle l'_{\bar{i}} r_{\bar{i}} \otimes i; SM \middle| V_i^{(1)} \middle| \Psi^{(0)} SM \right\rangle &= \sum_{t} \sum_{S'=|S-1/2|}^{S+1/2} \frac{\sqrt{2S'+1}}{\sqrt{2S+1}} h_{at}^{eff} \left\langle l'_{\bar{i}} r_{\bar{i}} S' \middle\| \hat{a}_t^{\dagger 1/2} \middle\| \Psi S \right\rangle \\ &+ \sum_{tuv} \sum_{S'=|S-1/2|}^{S+1/2} \frac{\sqrt{2S'+1}}{\sqrt{2S+1}} \left\langle l'_{\bar{i}} r_{\bar{i}} S' \middle\| \tilde{O}_{tuv}^{1/2} \right. \\ &\times \left. \| \Psi S \right\rangle \cdot (\boldsymbol{ti} \,|\, \boldsymbol{uv}). \end{aligned} \tag{B4}$$

[1]F. Jensen, *Introduction to Computational Chemistry* (John Wiley & Sons, New York, 1999).
[2]P. G. Szalay, T. Müller, G. Gidofalvi, H. Lischka, and R. Shepard, Chem. Rev. **112**(1), 108–181 (2012).
[3]K. Andersson, P. A. Malmqvist, B. O. Roos, A. J. Sadlej, and K. Wolinski, J. Phys. Chem. **94**(14), 5483–5488 (1990).
[4]K. Andersson, P.-A. Malmqvist, and B. O. Roos, J. Chem. Phys. **96**(2), 1218–1226 (1992).
[5]C. Angeli, R. Cimiraglia, S. Evangelisti, T. Leininger, and J. P. Malrieu, J. Chem. Phys. **114**, 10252 (2001).
[6]C. Angeli, R. Cimiraglia, and J. P. Malrieu, J. Chem. Phys. **117**, 9138 (2002).
[7]P. Celani and H.-J. Werner, J. Chem. Phys. **112**(13), 5546–5557 (2000).
[8]P. A. Malmqvist, A. Rendell, and B. O. Roos, J. Phys. Chem. **94**(14), 5477–5482 (1990).
[9]J. Olsen, B. O. Roos, P. Jo/rgensen, and H. J. r. A. Jensen, J. Chem. Phys. **89**(4), 2185–2192 (1988).
[10]G. K.-L. Chan and M. Head-Gordon, J. Chem. Phys. **116**, 4462 (2002).
[11]Ö. Legeza, J. Röder, and B. A. Hess, Phys. Rev. B **67**(12), 125114 (2003).
[12]U. Schollöwck, Rev. Mod. Phys. **77**(1), 259–315 (2005).
[13]J. Hachmann, W. Cardoen, and G. K.-L. Chan, J. Chem. Phys. **125**, 144101 (2006).
[14]K. H. Marti, I. M. Ondík, G. Moritz, and M. Reiher, J. Chem. Phys. **128**, 014104 (2008).
[15]Y. Kurashige and T. Yanai, J. Chem. Phys. **130**, 234114 (2009).
[16]S. Sharma, K. Sivalingam, F. Neese, and G. K.-L. Chan, Nat. Chem. **6**(10), 927–933 (2014).
[17]S. Wouters, T. Bogaerts, P. Van Der Voort, V. Van Speybroeck, and D. Van Neck, J. Chem. Phys. **140**(24), 241103 (2014).
[18]Y. Kurashige, G. K.-L. Chan, and T. Yanai, Nat. Chem. **5**, 660–666 (2013).
[19]S. R. White, Phys. Rev. Lett. **69**(19), 2863 (1992).
[20]S. R. White, Phys. Rev. B **48**(14), 10345 (1993).
[21]S. R. White and R. L. Martin, J. Chem. Phys. **110**, 4127 (1999).
[22]J. Hachmann, J. J. Dorando, M. Avilés, and G. K.-L. Chan, J. Chem. Phys. **127**(13), 134309 (2007).
[23]J. Chalupský, T. A. Rokob, Y. Kurashige, T. Yanai, E. I. Solomon, L. Rulíšek, and M. Srnec, J. Am. Chem. Soc. **136**(45), 15977–15991 (2014).
[24]Y. Kurashige, M. Saitow, J. Chalupský, and T. Yanai, Phys. Chem. Chem. Phys. **16**(24), 11988–11999 (2014).
[25]K. H. Marti and M. Reiher, Z. Phys. Chem. **224**(3–4), 583–599 (2010).
[26]T. V. Harris, Y. Kurashige, T. Yanai, and K. Morokuma, J. Chem. Phys. **140**(5), 054303 (2014).
[27]K. Boguslawski, K. H. Marti, Ö. Legeza, and M. Reiher, J. Chem. Theory Comput. **8**(6), 1970–1982 (2012).
[28]L. Freitag, S. Knecht, S. F. Keller, M. G. Delcey, F. Aquilante, T. B. Pedersen, R. Lindh, M. Reiher, and L. González, Phys. Chem. Chem. Phys. **17**(22), 14383–14392 (2015).
[29]Y. Ma, J. Wen, and H. Ma, J. Chem. Phys. **143**(3), 034105 (2015).
[30]Y. Kurashige and T. Yanai, J. Chem. Phys. **135**(9), 094104 (2011).
[31]M. Saitow, Y. Kurashige, and T. Yanai, J. Chem. Phys. **139**(4), 044118 (2013).
[32]M. Saitow, Y. Kurashige, and T. Yanai, J. Chem. Theory Comput. **11**(11), 5120–5131 (2015).
[33]S. Guo, M. A. Watson, W. Hu, Q. Sun, and G. K. Chan, J. Chem. Theory Comput. **12**(4), 1583–1591 (2016).
[34]T. Yanai, Y. Kurashige, W. Mizukami, J. Chalupský, T. N. Lan, and M. Saitow, Int. J. Quantum Chem. **115**(5), 283–299 (2015).
[35]T. Yanai and G. K.-L. Chan, J. Chem. Phys. **124**(19), 194106 (2006).
[36]T. Yanai, Y. Kurashige, E. Neuscamman, and G. K.-L. Chan, J. Chem. Phys. **132**(2), 024105 (2010).
[37]E. Neuscamman, T. Yanai, and G. K.-L. Chan, Int. Rev. Phys. Chem. **29**(2), 231–271 (2010).
[38]T. Yanai, Y. Kurashige, E. Neuscamman, and G. K.-L. Chan, Phys. Chem. Chem. Phys. **14**(21), 7809–7820 (2012).
[39]Y. Kurashige, J. Chalupský, T. N. Lan, and T. Yanai, J. Chem. Phys. **141**(17), 174111 (2014).
[40]S. Sharma and G. K.-L. Chan, J. Chem. Phys. **141**(11), 111101 (2014).
[41]S. Sharma and A. Alavi, J. Chem. Phys. **143**(10), 102815 (2015).
[42]E. Xu, D. Zhao, and S. Li, J. Chem. Theory Comput. **11**(10), 4634–4643 (2015).
[43]E. Xu and S. Li, J. Chem. Phys. **139**(17), 174111 (2013).
[44]A. Y. Sokolov and G. K.-L. Chan, J. Chem. Phys. **144**, 064102 (2016).
[45]E. D. Hedegård, S. Knecht, J. S. Kielberg, H. J. A. Jensen, and M. Reiher, J. Chem. Phys. **142**(22), 224108 (2015).
[46]T. Dresselhaus, J. Neugebauer, S. Knecht, S. Keller, Y. Ma, and M. Reiher, J. Chem. Phys. **142**(4), 044111 (2015).
[47]G. K.-L. Chan and S. Sharma, Annu. Rev. Phys. Chem. **62**(1), 465–481 (2011).
[48]S. Wouters and D. Van Neck, Eur. Phys. J D **68**, 272 (2014).
[49]G. K.-L. Chan, J. J. Dorando, D. Ghosh, J. Hachmann, E. Neuscamman, H. Wang, and T. Yanai, Front. Quantum Syst. Chem. Phys. **18**, 49–65 (2008).
[50]G. Moritz, B. A. Hess, and M. Reiher, J. Chem. Phys. **122**(2), 024107 (2005).
[51]G. Barcza, Ö. Legeza, K. Marti, and M. Reiher, Phys. Rev. A **83**(1), 012508 (2011).
[52]R. Olivares-Amaya, W. Hu, N. Nakatani, S. Sharma, J. Yang, and G. K.-L. Chan, J. Chem. Phys. **142**(3), 034102 (2015).
[53]E. R. Davidson, J. Comput. Phys. **17**(1), 87–94 (1975).
[54]C. Lanczos, J. Res. Nat. Bur. Stand. **45**, 252–282 (1950).
[55]S. Sharma and G. K.-L. Chan, J. Chem. Phys. **136**, 124121 (2012).
[56]K. G. Dyall, J. Chem. Phys. **102**, 4909 (1995).
[57]D. Ghosh, J. Hachmann, T. Yanai, and G. K.-L. Chan, J. Chem. Phys. **128**(14), 144117 (2008).
[58]D. Zgid and M. Nooijen, J. Chem. Phys. **128**(14), 144115 (2008).
[59]Y. Guo, K. Sivalingam, E. F. Valeev, and F. Neese, J. Chem. Phys. **144**(9), 094111 (2016).
[60]F. Neese, Wiley Interdiscip. Rev.: Comput. Mol. Sci. **2**(1), 73–78 (2012).
[61]F. Weigend and R. Ahlrichs, Phys. Chem. Chem. Phys. **7**(18), 3297–3305 (2005).
[62]D. R. Lide, *Handbook of Chemistry and Physics*, 90th ed. (CRC Press, Boca Raton, 2009).
[63]E. I. Solomon, F. Tuczek, D. E. Root, and C. A. Brown, Chem. Rev. **94**(3), 827–856 (1994).
[64]E. I. Solomon, U. M. Sundaram, and T. E. Machonkin, Chem. Rev. **96**(7), 2563–2606 (1996).
[65]J. A. Halfen, S. Mahapatra, E. C. Wilkinson, S. Kaderli, V. G. Young, L. Que, A. D. Zuberbühler, and W. B. Tolman, Science **271**(5254), 1397–1400 (1996).
[66]S. Mahapatra, J. A. Halfen, E. C. Wilkinson, G. Pan, X. Wang, V. G. Young, C. J. Cramer, L. Que, and W. B. Tolman, J. Am. Chem. Soc. **118**(46), 11555–11574 (1996).
[67]J. L. DuBois, P. Mukherjee, A. M. Collier, J. M. Mayer, E. I. Solomon, B. Hedman, T. D. P. Stack, and K. O. Hodgson, J. Am. Chem. Soc. **119**(36), 8578–8579 (1997).
[68]Z. Tyeklar, R. R. Jacobson, N. Wei, N. N. Murthy, J. Zubieta, and K. D. Karlin, J. Am. Chem. Soc. **115**(7), 2677–2689 (1993).
[69]R. R. Jacobson, Z. Tyeklar, A. Farooq, K. D. Karlin, S. Liu, and J. Zubieta, J. Am. Chem. Soc. **110**(11), 3690–3692 (1988).
[70]C. J. Cramer, A. Kinal, M. Włoch, P. Piecuch, and L. Gagliardi, J. Phys. Chem. A **110**(40), 11557–11568 (2006).
[71]C. J. Cramer, B. A. Smith, and W. B. Tolman, J. Am. Chem. Soc. **118**(45), 11283–11287 (1996).
[72]C. J. Cramer, M. Woch, P. Piecuch, C. Puzzarini, and L. Gagliardi, J. Phys. Chem. A **110**(5), 1991–2004 (2006).
[73]M. Flock and K. Pierloot, J. Phys. Chem. A **103**(1), 95–102 (1999).
[74]D. G. Liakos and F. Neese, J. Chem. Theory Comput. **7**(5), 1511–1523 (2011).